# Increasing nutrient fluxes and mixing regime changes in the eastern Arctic Ocean

Shultz, Kirsten; Lincoln, Ben; Povazhnyy, V; Rippeth, Tom; Lenn, Yueng-Djern; Janout, Markus; Alkire, Matthew; Scannell, Brian; Torres-Valdes, Sinhue

**Geophysical Research Letters**

*DOI:*
10.1029/2021GL096152

Published: 16/03/2022

Publisher's PDF, also known as Version of record

AGU ADVANCING EARTH AND SPACE SCIENCE

# Geophysical Research Letters

RESEARCH LETTER
10.1029/2021GL096152

**Key Points:**

- Nutrient fluxes are higher in the western compared with the eastern Laptev Sea
- Episodic mixing above the slope might significantly contribute to Pan-Arctic vertical nitrate supply
- In the central Laptev Sea, a thinning halocline and shoaling Atlantic Water indicate an emerging regime shift in line with Atlantification

**Correspondence to:**

K. Schulz,
kiki.schulz@utexas.edu

**Citation:**

Schulz, K., Lincoln, B., Povazhnyy, V., Rippeth, T., Lenn, Y.-D., Janout, M., et al. (2022). Increasing nutrient fluxes and mixing regime changes in the eastern Arctic Ocean. *Geophysical Research Letters*, *49*, e2021GL096152. https://doi.org/10.1029/2021GL096152

Received 13 SEP 2021
Accepted 14 FEB 2022

**Author Contributions:**

**Conceptualization:** K. Schulz, B. Lincoln, T. Rippeth, Y.-D. Lenn, S. Torres-Valdés
**Data curation:** K. Schulz
**Formal analysis:** K. Schulz, B. Lincoln, V. Povazhnyy
**Funding acquisition:** Y.-D. Lenn, M. Janout, M. Alkire, S. Torres-Valdés
**Investigation:** K. Schulz, V. Povazhnyy
**Methodology:** K. Schulz, B. Lincoln, V. Povazhnyy, M. Alkire
**Project Administration:** Y.-D. Lenn, M. Janout
**Resources:** V. Povazhnyy, M. Janout, M. Alkire
**Supervision:** Y.-D. Lenn, M. Janout
**Validation:** K. Schulz
**Visualization:** K. Schulz
**Writing – original draft:** K. Schulz, V. Povazhnyy, T. Rippeth, M. Janout, B. Scannell, S. Torres-Valdés



# Increasing Nutrient Fluxes and Mixing Regime Changes in the Eastern Arctic Ocean

**K. Schulz[1,2], B. Lincoln[3], V. Povazhnyy[4], T. Rippeth[3], Y.-D. Lenn[3], M. Janout[1], M. Alkire[5], B. Scannell[3], and S. Torres-Valdés[1]**

[1]Alfred Wegener Institute, Helmholtz Centre for Polar and Marine Research, Bremerhaven, Germany, [2]Now at: Oden Institute for Computational Engineering and Sciences, The University of Texas at Austin, Austin, TX, United States, [3]School of Ocean Sciences, Bangor University, Bangor, UK, [4]State Scientific Center of the Russian Federation Arctic and Antarctic Research Institute, St. Petersburg, Russia, [5]University of Washington, Seattle, WA, USA

**Abstract** Primary productivity in the Arctic Ocean is experiencing dramatic changes linked to the receding sea ice cover. The vertical transport of nutrients from deeper water layers is the limiting factor for primary production. Here, we compare coincident profiles of turbulence and nutrients from the Siberian Seas in 2007, 2008, and 2018. In all years, the water column structure in the upstream region of the Arctic Boundary Current promotes upward nutrient transport, in contrast to the regions further downstream, and there are first indications for an eastward progression of these conditions. In summer 2018, strongly enhanced vertical nitrate flux and primary production above the continental slope were observed, likely related to a remote storm. The estimated contribution of these elevated fluxes above the slope to the Pan-Arctic vertical nitrate supply is comparable with the basin-wide transport, and is predicted to increase with declining sea ice cover in the future.

**Plain Language Summary** Microscopic algae, growing in the sunlit surface layer of the ocean, provide food for other species and form the basis of the ecosystem. In the Arctic Ocean, their growth is limited by the availability of nutrients. The main source of these nutrients are waters entering from the Atlantic and Pacific Oceans. These nutrient-rich waters reside far below the sunlit zone, and vertical mixing is required to bring them upwards to support algal growth. With rapidly declining summer sea ice and changes in the ocean layering, these mixing processes might substantially change. Changes are considered most likely in the region of the steep slopes in the Siberian Seas. To investigate this, we analyze nutrient and mixing measurements in this region from 2007, 2008, and 2018. In 2018, we observed strong mixing, which is connected to ice free conditions and a process that has only recently been described. This strong mixing only happens at the narrow, steep slope region, but might supply the same amount of nutrients to the surface zone as the weak mixing over the much larger area of the deep basins.

## 1. Introduction

The Arctic Ocean seasonal sea ice cover has dramatically declined in recent decades (Stroeve et al., 2008), and the 14 lowest minimum sea ice extents on record have been observed in the past 14 years. Net primary productivity (NPP) has increased by at least 30% (1998–2012, Arrigo & van Dijken, 2015). In the Arctic Ocean, NPP and particularly sub-surface blooms, are limited by the depletion of nitrate (Tremblay et al., 2015). The contribution of riverine nitrate to the Arctic ecosystem is regionally small, negligible on the pan-Arctic scale (Fouest et al., 2013), and the primary source of nitrate is the nutrient-rich Atlantic and Pacific Water (Torres-Valdés et al., 2013). In large parts of the Arctic Ocean, these water masses are situated at intermediate depths, isolated from the surface (e.g., Rudels, 2012; Schauer et al., 1997). Vertical mixing processes are critical for nutrient delivery to support primary productivity occurring in the euphotic zone (Arrigo & van Dijken, 2015; Tremblay et al., 2015; Ardyna et al., 2014; Fouest et al., 2013).

The observed increase in NPP varies regionally with a particularly strong response in the eastern Arctic Ocean. The highest increase in NPP of more than 110% was observed in the Laptev Sea shelf break region (Arrigo & van Dijken, 2015). This is consistent with the notion that continental slopes are key regions for enhanced vertical mixing (Fer et al., 2020; Lenn et al., 2011; Renner et al., 2018; Rippeth et al., 2015; Schulz, Janout, et al., 2021). North of Svalbard, where the Atlantic Water (AW) is located relatively close to the surface, storm events can strongly enhance vertical transport and bring nutrient-rich waters closer to the surface (Meyer et al., 2017).

10.1029/2021GL096152

**Writing – review & editing:** K. Schulz, B. Lincoln, V. Povazhnyy, T. Rippeth, Y.-D. Lenn, M. Janout, M. Alkire, B. Scannell

Further to the east, along the boundary current pathway, at the shelf break in the Siberian Seas, the AW is situated deeper in the water column, and the vertical transfer of nutrients to the surface by mixing related to storm events is hindered by a perennial halocline. While enhanced mid-water dissipation attributed to tidally-generated unsteady lee waves has been observed over Arctic continental slopes (Fer et al., 2015, 2020; Padman et al., 1992; Rippeth et al., 2017), the cross-slope tidal flow in the Siberian Seas is weak, with low levels of tidal conversion and mixing (Fer et al., 2020; Rippeth et al., 2015). Energy conversion mechanisms to generate enhanced mixing from larger scale flow anomalies have just recently been described (Schulz, Büttner, et al., 2021). In addition, over the past decade and a half, warming (Barton et al., 2018) and shoaling of the AW (Polyakov et al., 2017, 2020) together with a weakening of the overlying halocline have led to significantly increased ventilation of the AW (Polyakov et al., 2020; Schulz, Janout, et al., 2021). Hence, the largely unresolved nutrient dynamics in the Siberian sector might be in transition, along with the ongoing oceanographic regime shift.

Here, we compare profiles of turbulent dissipation rates and nitrate fluxes in September/October 2007, October 2008, and August/September 2018, and aim to evaluate whether nutrient fluxes are increasing above the continental shelf break in the Siberian sector of the Arctic Ocean. We assess the changes in the water column structure and nitrate distribution between the campaigns (Section 3), estimate an average nitrate flux from the loss of nitrate in the upper 250 m along the AW pathway (Section 4), and present the local nitrate fluxes derived from nitrate and turbulent dissipation rate profiles (Section 5).

## 2. Methods

In summer 2018, vertical conductivity, temperature, depth (CTD, SBE9+, Seabird Scientific) and Submersible Ultraviolet Nitrate Profiler (SUNA) nitrate concentration profile measurements were performed in the Laptev and East Siberian Seas (Figure 1a). At 22 of 85 stations, additional measurements with a microstructure profiler (MSS, MSS90L, Sea and Sun Technology, Germany) were carried out after the CTD casts, to obtain vertical profiles of turbulent dissipation rates (see Schulz, Janout, et al., 2021, for details on instrumentation and post-processing). Both CTD and MSS were equipped with fluorescence sensors (WETLabs ECO-FLNTU and Turner Designs Cyclops 7, respectively). The CTD was further equipped with a dissolved oxygen sensor (SBE43, Seabird Scientific), which was calibrated against Winkler measurements. Conditions were mostly ice-free, only the easternmost transects VII and VIII were carried out in the marginal ice zone (see Tarasenko et al., 2021, for details).

The SUNA measures the ultraviolet (217–240 nm) absorbance of seawater across the probe's 1 cm path length approximately once per second, to estimate nitrate concentration. Bromide absorption spectra were estimated and removed using in-situ temperature and salinity data, and a linear baseline correction was applied to account for absorption by colored dissolved organic matter (Sakamoto et al., 2009). SUNA nitrate concentrations were calibrated against nitrate concentrations measured from seawater samples, and the uncertainty was estimated to be 0.7 mmol $m^{-3}$. Additional processing information is provided in the data publication. All CTD and SUNA data were averaged to 2 dbar vertical resolution.

Primary production was determined by oxygen modification directly after sampling in 125 ml white glass bottles with optical oxygen sensor spots installed. Respiration was determined in foil-wrapped bottles of the same volume. The bottles were incubated in a thermo-stabilized luminostate at 100 μE $m^{-2}$ $s^{-1}$ photosynthetically active radiation (PAR) at 1°C (surface layer) and 16 μE $m^{-2}$ $s^{-1}$ PAR at −0.9°C (chl-a maximum layer). Initial $O_2$ concentration was determined after a 3 hr acclimation period, and then additional $O_2$ determinations were made every 3–6 hr (depending on initial chl-a concentration) to track production. Samples for initial and final chl-a concentrations were filtered onto 25 mm GF/F filters and stored frozen (−20°C) until extraction with 90% acetone on TD700 fluorimeter without acidification (see Campbell et al., 2016, for details). To convert from measured mg C $m^{-3}$ $h^{-1}$ to mg C $m^{-2}$ $d^{-1}$, an average Secci depth of 15 m, based on five measurements, and 16 hr of sunlight per day were used.

SUNA and primary productivity data are only available for 2018. In 2007 and 2008, CTD (SBE19+) casts, nutrient concentration measurements from discrete water samples, and microstructure observations using a free-falling, tethered Vertical Microstructure Profiler (VMP500, Rockland Scientific Instruments) were carried out (Figure 1a). Details on the nutrient sampling, instrumentation and post-processing can be found in Lenn

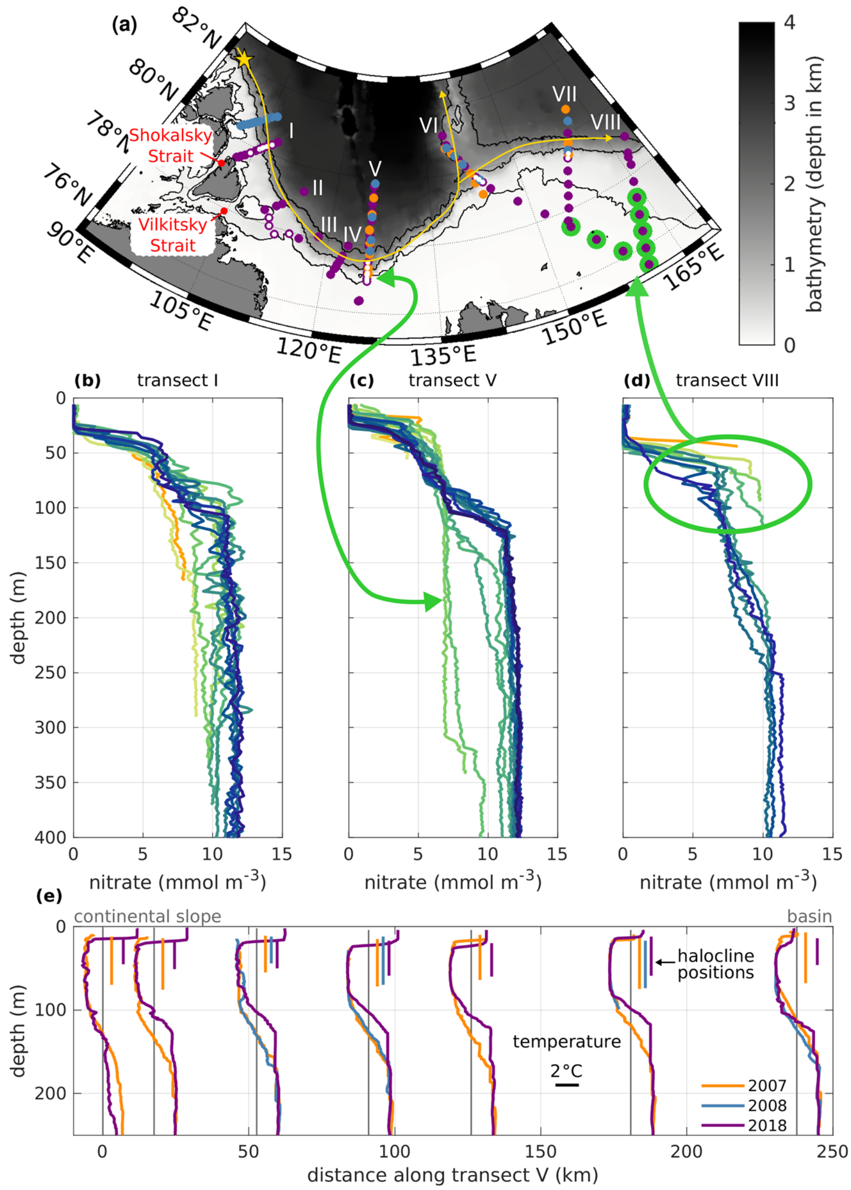


**Figure 1.** (a) Topographic map of the study region, with dots indicating VMP and discrete nutrient sampling stations from 2007 (orange), 2008 (blue), SUNA profiles (purple), and MSS profiles (small white) from 2018. A yellow star indicates the mooring position, black lines the 100, 1,000, and 2,000 m isobath, yellow arrows indicate the Boundary Current pathway. (b)–(d) Example 2018 nitrate profiles, colors indicate distance along respective transect, from shelf (orange) to basin (blue). Green arrow indicate the position of atypically homogeneous (transect V) and high near-bottom (transect VIII) nitrate concentrations on the map. (e) Temperature profiles and the halocline extent (vertical lines) from repeated stations on transect V (2007 = orange, blue = 2008, purple = 2018).

et al. (2009); Abrahamsen et al. (2009); Rippeth et al. (2015); Polyakov et al. (2019), and in the expedition reports (https://uaf-iarc.org/nabos-cruises/).

Nitrate fluxes across the nitracline were calculated following Randelhoff et al. (2016), as

$$F_N = 0.2\varepsilon \frac{\rho}{g}\frac{\partial N}{\partial \sigma_\theta},$$

where $\varepsilon$ is the turbulent dissipation rate in W kg$^{-1}$, N is the nitrate concentration in mmol m$^{-3}$, $\rho = 1{,}027$ kg m$^{-3}$ is the density of sea water, $\sigma_\theta$ is the potential density anomaly and $g = 9.81$ m s$^{-2}$ is the gravitational acceleration.

$F_N$ is given in units of mmol m$^{-2}$ d$^{-1}$, positive values correspond to an upward flux. We define the upper bound of the nitracline as the first depth where nitrate concentrations exceed 20% of the difference in concentration between maximum surface (0–8 m) and deep reference (profile maximum) concentration, and the lower bound where the concentrations exceed 80% of this concentration difference. The nitrate gradient $\frac{\partial N}{\partial \sigma_\theta}$ is estimated as a linear regression against density over the nitracline range. For 2007 and 2008, nitrate concentrations from the discrete samples between 30 and 200 m depth were used to calculate the nitrate gradient. Turbulent dissipation rates $\varepsilon$ were averaged over the nitracline density range, to avoid biases by vertical isopycnal displacement. The estimated nitrate fluxes are insensitive to the exact choice of the nitracline depth, for example, a shallower upper nitracline bound, defined as the first depth were nitrate concentration exceed 10% (as opposed to 20% used in this study) of the previously defined concentration difference, results in an average nitrate flux difference of less than 2%.

An upward-looking 75 kHz Acoustic Doppler Current Profiler (ADCP, Teledyne RD Instruments, US) was moored at 82°06.28' N, 094°46.34 E (~2,000 m water depth, Figure 1a), from September 2015 to August 2018, at a depth of 481 m, and sampled velocity profiles with 8 m bins and 90 min ensembles. We use the depth-averaged current between 50 and 300 m in the main current direction (+20°) to calculate the propagation time of the Arctic Boundary Current (see Section 4). Distances between transects are calculated along the 1,000 m isobath. To account for the deceleration of the boundary current speed along the domain (Pnyushkov et al., 2015), we assume a linear decrease of the current magnitude to half its propagation speed between the position of the mooring and the Lomonosov Ridge, represented by transect VI (see Schulz, Janout, et al., 2021, for details and a discussion about uncertainties).

## 3. Changes in Water Column Structure and Nitrate Distribution

The water column structure in summer 2018 comprised a warm and relatively fresh surface mixed layer (SML, lower bound identified by a change of water density of 0.125 kg m$^{-3}$ relative to the surface value), with highest SML temperatures and lowest salinities found on the inner shelf (Schulz, Janout, et al., 2021; Tarasenko et al., 2021, for details). Below the SML, a near-freezing halocline layer extended to a depth of around 60 m in the western part of the study region, and up to 90 m depth in the eastern part (see Schulz, Janout, et al., 2021, for water mass definition). Warmer AW (>0°C) transported with the Arctic Boundary Current resides at intermediate depths (e.g., Figure 1e). Vertical mixing successively erodes the top of the AW layer during its propagation, deepening the warm core depth from 120 to 250 m and causing a decrease in maximum temperature, from 2.2°C on transect I to 1.3°C on transect VIII (data not shown).

Comparing the 2007–2008 and 2018 data, the average vertical extent of the cold halocline layer in the central Laptev Sea (transect V, 126°E, based on seven repeated profiles, see Figure 1e) has decreased by 20 m, the thermocline is sharper and the AW is situated higher in the water column. This observed decrease in halocline thickness exceeds the standard deviation of the halocline thickness (15 m) in the Amundsen Basin (Bourgain & Gascard, 2011). A thinning halocline is consistent with Atlantification, that is, the eastward progression of oceanic conditions typically found in the Svalbard and Barents Sea region, where the thin halocline is seasonal and the AW resides close to the surface (Polyakov et al., 2017). The other two repeated transects VI (5 revisited stations) and VII (3 revisited stations) are located several 100 km further east than transect V, downstream of the Atlantic Water pathway. There, water column structure was comparable in all sampled years, hinting that Atlantification has not reached this area yet.

At most stations in 2018, nitrate was depleted in the SML, and concentrations increased with depth (Figures 1b–1d). A subsurface peak in fluorescence (e.g., Figure 3e in Section 5) suggests that algae reside in the photic zone below the SML, where nitrate concentration were above zero. Nitrate concentrations were highest below the AW temperature maximum at 10.5–12.3 mmol m$^{-3}$. Above the continental slope, where nutrient-rich AW is mixed with nutrient-poor shelf water (Schulz, Janout, et al., 2021), the nitrate concentrations were generally lower compared to profiles measured further offshore (e.g., Figure 1b). The discrete sample nitrate concentrations from both 2007 and 2008 exhibit the same vertical pattern as the measured profiles in 2018, but nitrate concentrations in the AW layer were slightly higher (10.8–14.8 mmol m$^{-3}$, data not shown) than in 2018.

At the shallow stations near Vilkitsky Strait on transects II and III (sampled August 27/28, 2018), no distinct SML was present and elevated nitrate concentrations extended up to the surface. In the marginal ice zone, on

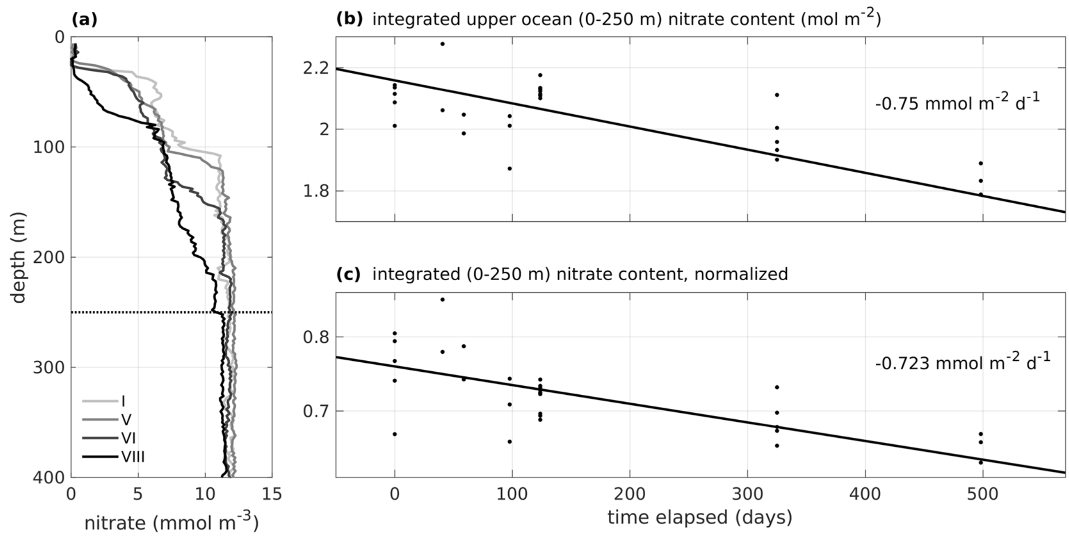


**Figure 2.** Summer 2018: (a) Selected nitrate concentration profiles with transect number indicated in gray scale, (b) integrated upper (0–250 m) ocean nitrate content (mol $m^{-2}$), (c) normalized upper ocean nitrate content, relative to the elapsed propagation time of the boundary current along its pathway.

transects VII and VIII (September 9–17, 2018), nitrate concentrations in the SML were still slightly above zero (0.5–1 mmol $m^{-3}$, e.g., Figure 1d). Fluorescence values at all these stations were maximum at the surface. Furthermore, in the near-bottom layer of the easternmost shelf stations (indicated with a green circle and green dots in Figures 1a and 1d) nitrate concentrations were high (up to 10 mmol $m^{-3}$) in 2018. An unusual vertical nitrate distribution was found at two stations above the continental slope (transect V, 2018, green arrow in Figures 1a and 1b), a consequence of previously identified strong local vertical mixing at this location (Schulz, Büttner, et al., 2021, discussed in detail in Section 5).

## 4. Nitrate Drawdown Along the Arctic Boundary Current Pathway

Before presenting directly calculated nitrate fluxes in the next section, we first estimate an average nitrate drawdown in waters advected with the Arctic Boundary Current. For this purpose we calculated the upper ocean nitrate content for each profile observed, by integrating the nitrate concentration between the surface and 250 m depth. Below 250 m, nitrate concentrations exhibit no variability along the boundary current pathway (Figure 2a). Profiles close to the continental slope, influenced by local lateral mixing with shelf waters and without well-defined AW core, were excluded from the calculation.

Individual nitrate content estimates from each transect were plotted against the successive progression time of the boundary current between the transects, starting with zero time elapsed on transect I and reaching the last transect VIII after ~500 days (Figure 2b). The progression time was calculated from contemporaneous current meter data as described in Section 2. To exclude interannual and seasonal variability in the upstream AW nitrate concentrations, the calculations were repeated using the upper ocean nitrate content, normalized with the corresponding average nitrate concentration in the AW (Figure 2c). The slope of the respective linear regression then gives an average nitrate drawdown from the upper ocean per time unit, based on data spanning a boundary current propagation time of approximately 500 days.

Both methods yield similar annual average nitrate drawdown rates of −0.75 (non-normalized) and −0.72 mmol $m^{-2}$ $d^{-1}$ (normalized), corresponding to approximately −270 mmol $m^{-2}$ per year. Uncertainties in these estimates arise from the limited knowledge of the spatial variability of the boundary current propagation speed and the exact propagation pathway, the sparse data coverage, and the seasonality of nitrate consumption (a detailed uncertainty discussion can be found in Schulz, Janout, et al., 2021). Moreover, the neglect of local remineralization and the subsequent recycling of nutrients likely results in an underestimation of the average nitrate drawdown. Hence, we will treat the calculated nitrate drawdown rate as an order of magnitude estimate of $\mathcal{O}(-1)$ mmol $m^{-2}$ $d^{-1}$.

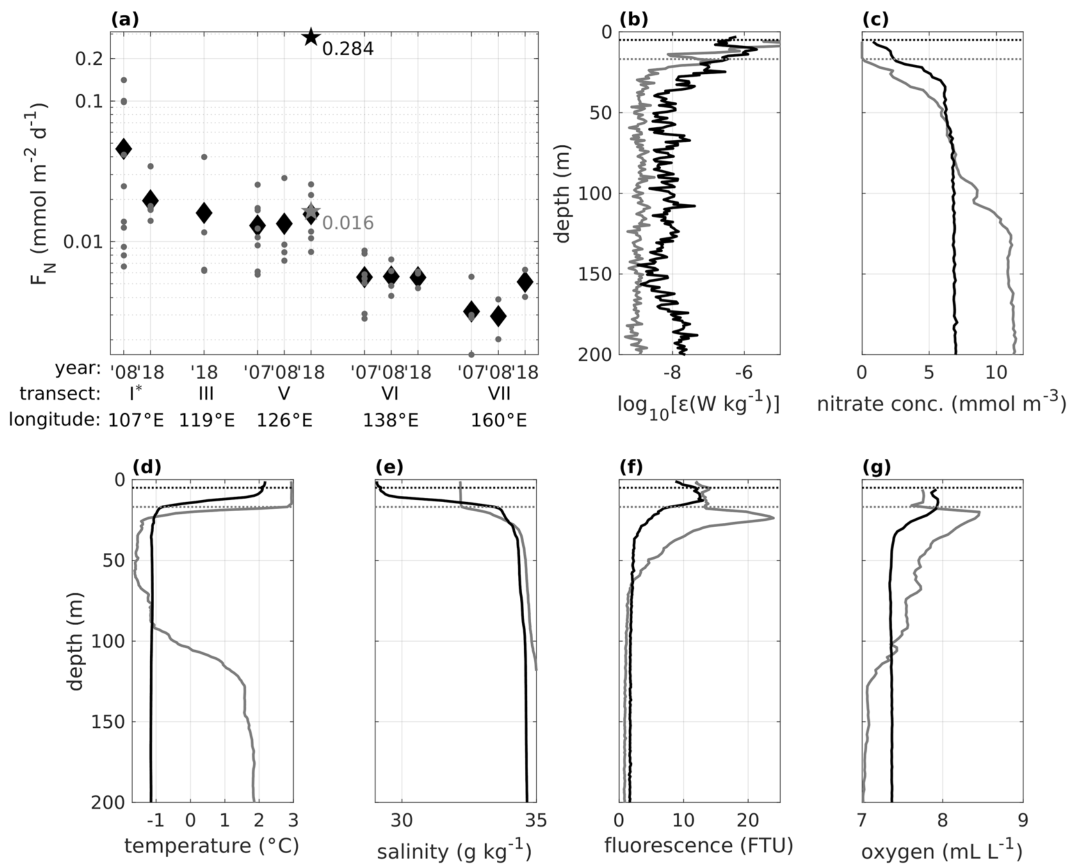


**Figure 3.** (a) Individual (dots and stars) and average (diamonds, value marked with black star excluded) nitrate fluxes (mmol m$^{-2}$ d$^{-1}$, logarithmic axis) per transect and sampling year. Vertical profiles of (b) dissipation rate (W kg$^{-1}$), (c) nitrate concentration (mmol m$^{-3}$), (d) potential temperature (°C), (e) absolute salinity (g kg$^{-1}$), (f) fluorescence (FTU), and (g) dissolved oxygen (mL L$^{-1}$) for the highly turbulent and a representative reference station on transect V (2018), marked with stars in (a) (black = 380 m, gray = 1,710 m water depth, 46 km apart, both sampled within 25 hr). Dashed lines in (b)–(g) indicate the depth of the surface mixed layer. *Transect I was performed upstream and downstream of Shokalsky Strait in 2008 and 2018, respectively.

Under the assumption that the only nitrate sink is consumption in the near-surface layer, this nitrate drawdown rate corresponds to the rate at which nitrate is supplied to the surface layer.

## 5. Vertical Nitrate Transport

Most vertical nitrate fluxes calculated from our data set range from 0.004 to 0.04 mmol m$^{-2}$ d$^{-1}$ (Figure 3a). West of 130° E, where the nutrient-rich AW is relatively shallow and the topography is more irregular in the vicinity of straits, the average nitrate flux is higher than in the eastern part of the study region. One exceptionally large flux of 0.29 mmol m$^{-2}$ d$^{-1}$ was observed on transect V in 2018 (green arrow in Figures 1a and 1c; black star in Figure 3a). Mid-water turbulent dissipation rates at this station are up to two orders of magnitude larger than the typical values of 10$^{-9}$ W kg$^{-1}$ found in this region (Schulz, Janout, et al., 2021). This intense mixing episode has been attributed to the dissipation of an unsteady lee wave associated with a passing continental shelf wave linked to a farfield storm (Schulz, Büttner, et al., 2021). The strong mixing episode redistributed nitrate, dissolved oxygen, fluorescent material, temperature and salinity (Figures 3c–3g, only the relevant upper 200 m are shown), leading to homogeneous concentrations between 30 and 300 m water depth. The observed decrease in nitrate concentration toward the surface may have been caused (at least partially) by local consumption in the euphotic zone. The chlorophyll maximum here was situated close to the surface, and measured surface net

10.1029/2021GL096152

**Table 1**
*Gross (GPP, g C $m^{-2}$ $d^{-1}$) and Net (NPP, g C $m^{-2}$ $d^{-1}$) Primary Productivity From Summer 2018*

| Position | Depth | GPP | NPP | Depth | GPP | NPP | Comment |
|---|---|---|---|---|---|---|---|
| 81.96°N 94.55°E | Surface | 0.3648 | 0.1848 | 25 m | 1.1016 | 0.8688 | North of Severnaya Zemlya |
| 82.56°N 95.55°E | | | | 10 m | 3.0768 | 2.7600 | North of Severnaya Zemlya |
| 79.16°N 100.29°E | Surface | 0.8136 | −0.3696 | | | | Within Shokalsky Strait |
| 79.14°N 100.58°E | Surface | 0.2592 | 0.1752 | | | | Within Shokalsky Strait |
| 79.33°N 100.76°E | Surface | 0.5232 | −0.2904 | | | | Within Shokalsky Strait |
| 79.50°N 102.86°E | surface | 0.9168 | −0.0072 | | | | Transect I |
| 80.01°N 105.71°E | | | | 20 m | 0.8232 | 0.4032 | Transect I |
| 77.80°N 117.00°E | surface | 0.5400 | 0.1632 | 25 m | 0.0096 | −0.3096 | Transect III |
| 77.03°N 121.05°E | | | | 16 m | 0.1104 | −0.0984 | Transect IV |
| 77.34°N 121.70°E | surface | 0.2904 | −0.0864 | 20 m | 1.1640 | 0.2448 | Transect IV |
| 76.00°N 126.01°E | | | | 20 m | 0.2976 | 0.1512 | Transect V |
| **77.16°N 125.98°E** | **surface** | **0.7728** | **0.4680** | **20 m** | **0.4296** | **0.1776** | Transect V |
| 78.48°N 125.99°E | surface | 1.0680 | −0.0648 | 30 m | 0.8400 | 0.1320 | Transect V |
| 79.74°N 125.96°E | surface | 0.4176 | −0.8784 | 20 m | 0.4344 | 0.3768 | Transect V |
| 79.97°N 126.18°E | | | | 30 m | 0.9456 | −0.2472 | Transect V |
| 76.60°N 143.95°E | surface | 1.3080 | 0.2664 | | | | On shelf |
| 79.60°N 143.95°E | surface | 1.1712 | −0.3936 | 20 m | 1.9104 | −0.5544 | Transect VI |
| 76.19°N 158.90°E | surface | 0.4656 | −0.0096 | 20 m | 1.3536 | 0.4704 | On shelf |
| | | | | 47 m | – | 1.1688 | On shelf |
| 79.52°N 158.51°E | surface | 0.0192 | −0.0408 | 20 m | 0.4512 | 0.1320 | Transect VII |
| 80.51°N 167.20°E | surface | 0.2256 | −0.3624 | 20 m | 0.6336 | 0.2424 | Transect VII |
| 72.83°N 63.44°E | surface | 0.1344 | −0.7344 | | | | Kara Sea |

*Note.* Data from the highly turbulent position is printed in bold face.

primary production was 0.47 g C $m^{-2}$ $d^{-1}$ (Table 1, bold line), approximately four times the value averaged over all performed measurements of 0.12 g C $m^{-2}$ $d^{-1}$.

Turbulent mixing is, however, highly intermittent, and the measured nitrate flux of 0.29 mmol $m^{-2}$ $d^{-1}$ only provides a snapshot of the dynamics during the mixing event. To assess the total nitrate supply to the approximately 50 m deep euphotic zone (Demidov et al., 2020) during the mixing event, we estimate the upper ocean (0–50 m) excess nitrate content at the high-turbulence station, relative to a representative reference profile 46 km further offshore on the same transect (black and gray profile, Figure 3c). This integrated nitrate concentration difference of approximately 80 mmol $m^{-2}$ omits nitrate that has already been consumed or removed by nitrification, and is hence a lower bound. As an upper bound, we assume a constant nitrate concentration of 6 mmol $m^{-3}$ in the top 50 m. Relative to the representative reference profile, this amounts to an excess concentration of approximately 180 mmol $m^{-2}$. In a previous study, it was found that continental shelf wave-induced mixing episodes occur approximately 8 times per year (based on data from 2015 to 2018, see Schulz, Büttner, et al., 2021). Based on the estimated lower and upper bound of the nitrate contribution during one mixing event, eight events per year would amount to an average annual flux of 1.8–3.9 mmol $m^{-2}$ $d^{-1}$. While this average nitrate flux is high compared to the flux estimated via the annual nitrate loss (Section 4), its spatial extent is confined. Only at the neighboring stations on the transect (6 km further offshore and 7 km further onshore), there is a comparable water column structure and vertical nitrate distribution, but no enhanced levels of mid-water turbulence was found. Enhanced surface nitrate concentrations were therefore not sustained by high vertical fluxes, but might have promoted primary production at a stage where surface nutrient concentrations are already low for a limited period of time. Hence, we suspect that episodic mixing events can boost primary production over a cross-slope distance of 10–20 km.

What is the relative contribution of episodic, strong mixing above the slope and how does it compare to the steady, but low, vertical nitrate transport over the larger area of the basin? Taking transect V at 126°E as a representative slice of the Arctic Ocean, an annual average nitrate flux of 2 mmol $m^{-2}$ $d^{-1}$ over a 10 km cross-slope distance at the upper slope amounts to the same supply as an average flux of 0.02 mmol $m^{-2}$ $d^{-1}$ over the approximately 1,000 km distance from the upper slope to the north pole. The contributions to the surface nitrate supply from the episodic mixing over the slope area and the weak mixing over the large basin might therefore be comparable. Similar strong mixing events driven by continental shelf waves are linked to ice-free conditions, and their contribution to the pan-Arctic nutrient supply will likely increase with receding ice cover in the future (Schulz, Büttner, et al., 2021).

The average summer vertical nitrate fluxes presented in this section of 0.04 mmol $m^{-2}$ $d^{-1}$ (including the estimated contribution from episodic mixing at the slope) can be contrasted with the estimated long-term mean nitrate drawdown of $\mathcal{O}(-1)$ mmol $m^{-2}$ $d^{-1}$ (Section 4). If summer vertical nitrate fluxes were the principal supply mechanism for nitrate to the euphotic zone, the average nitrate flux would roughly balance the average annual nitrate drawdown. The measured summer vertical fluxes are, however, considerably smaller, pointing to important, yet unresolved mechanisms for the transport of nitrate from deeper layers to the euphotic zone. These mixing processes might include tidally-driven mixing in the turbulent near-bottom layer at the upper slope (Lenn et al., 2011; Schulz, Janout, et al., 2021), the role of filaments and eddies for enhanced mixing in the vicinity of the boundary current and in the central basins (MacKinnon et al., 2021), or brine-driven convection during the freezing season. More observations are needed to conclusively understand Arctic nutrient transport dynamics, and the contribution of episodic mixing events.

## 6. Summary and Perspectives

Based on data from three hydrographic surveys carried out in 2007, 2008, and 2018, we assess recent changes in summer water column structure and oceanic nitrate supply in the Siberian Seas. In the western part of the Laptev Sea, the halocline is thinner and the AW is situated shallower, compared to further downstream of the boundary current. Consequently, vertical nitrate fluxes were higher in the west than in the east in all sampled years (Figure 3a). In the central Laptev Sea, a thinning halocline and a shallower AW layer over the 10 year time between the expeditions underlines the eastward progression of Atlantic-influenced conditions (Polyakov et al., 2017), that is, the transition toward a seasonal rather than perennial halocline. While more observations are needed to confirm this emerging trend, it is likely that an eastward shift of hydrographic conditions entails a regional increase in vertical nutrient fluxes. This implies that nutrient fluxes in the east may increase toward the present levels observed in the western Laptev Sea in response to Atlantification.

In addition, the key processes for vertical nitrate transport might have changed substantially. For the first time, strongly enhanced nitrate fluxes associated with a mixing event above the continental slope were observed in summer 2018. These episodic mixing events provide an explanation for observed elevated nutrients inventories above the Siberian shelf break (Randelhoff et al., 2020), where tidal velocities and levels of tidal conversion are relatively low (Rippeth et al., 2015). Their contribution to vertical nitrate supply may be approximately equal to the steady, but weak turbulent fluxes over the entire Siberian Sea area. Similar events have probably taken place in the past, but their occurrence has been linked to ice-free conditions in the Laptev Sea, and their frequency has likely increased with progressing sea ice reduction (Schulz, Büttner, et al., 2021). Assuming that this trend continues, we may expect a further increase in the relative importance of episodic boundary mixing events to the total Pan-Arctic vertical nutrient supply. However, the gap between the average measured nitrate flux and that required to balance the observed decrease in upper ocean nitrate content along the AW pathway points to the presence of additional, unresolved mixing processes. In particular, the role of frictional mixing in the near-bottom layer and the transport dynamics in the ice-covered season require further attention.

Our findings support the hypothesis that the increased net primary production in the Arctic continental slope region is supported by increased vertical fluxes of nutrients from the AW layer. Atlantification and declining sea ice cover are likely to amplify turbulent vertical transport, above the continental slope and potentially in the deeper basin, via both cross-slope lateral advection and a thinning of the halocline. These changes in the mixing regime, and hence vertical nutrient supply, bear the potential to strongly affect Arctic primary production, the ecosystem and organic carbon sequestration.

## Data Availability Statement

Hydrographic data sets used in this study are available at Alkire, (2019) Janout et al., (2020).

**Acknowledgments**

The expedition in summer 2018 aboard *Akademik Tryoshnikov* was carried out as a jointly organized research activity between the US-Russian NABOS (Nansen and Amundsen Basin Observational System) program and the German-Russian CATS (Changing Arctic Transpolar System) project as part of the "System Laptev Sea" partnership. The expeditions in 2007 aboard the *Viktor Buynitsky* and 2008 abord the *Kapitan Dranitsyn* were a joint effort between then Arctic Synoptic Basin-wide Oceanography (ASBO) and NABOS projects. We would like to thank Heidi Kassens, Igor Polyakov, Sheldon Bacon, Seymour Laxon and the organizers, crew and participants of all cruises. We also thank the three anonymous reviewers, who greatly helped to improve the manuscript. Financial support was received from the German Federal Ministry for Science and Education (BMBF) and the Ministry of Science and Higher Education of the Russian Federation as part of the Changing Arctic Transpolar System (CATS, Grant Nos. 03F0776, project RFMEFI61619X0108), as well as for the NERC-BMBF-funded PEANUTS-project (Grant No. 03F0804A). Alkire acknowledges funding from the National Science Foundation (PLR-1203146 AM003) and the National Oceanic and Atmospheric Administration (NA15OAR4310156). SUNA data was collected under the support of NSF grants OPP-1203146 (awarded to Matthew Alkire and James Morison) and OPP-1203473 (awarded to Igor Polyakov, Vladimir Alexeev, Robert Rember, and Vladimir Ivanov). Figure 1a was produced using the m_map matlab toolbox (Pawlowicz, 2000). Open access funding enabled and organized by Projekt DEAL.

## References

Abrahamsen, E. P., Meredith, M. P., Falkner, K. K., Torres-Valdes, S., Leng, M. J., Alkire, M. B., et al. (2009). Tracer-derived freshwater composition of the Siberian continental shelf and slope following the extreme Arctic summer of 2007. *Geophysical Research Letters*, *36*(7), a–n. https://doi.org/10.1029/2009GL037341

Alkire, M. (2019). Ocean conductivity, temperature, density (CTD), oxygen, and nitrate profiles, Eurasian and Makarov basins, Arctic Ocean, 2013–2018. [Dataset]. Arctic Data Center. Retrieved from https://arcticdata.io/catalog/view/https://doi.org/10.18739/A24X54G9W

Ardyna, M., Babin, M., Gosselin, M., Devred, E., Rainville, L., & Tremblay, J.-É. (2014). Recent Arctic Ocean sea ice loss triggers novel fall phytoplankton blooms. *Geophysical Research Letters*, *41*(17), 6207–6212. https://doi.org/10.1002/2014GL061047

Arrigo, K. R., & van Dijken, G. L. (2015). Continued increases in Arctic Ocean primary production. *Progress in Oceanography*, *136*, 60–70. https://doi.org/10.1016/j.pocean.2015.05.002

Barton, B. I., Lenn, Y.-D., & Lique, C. (2018). Observed Atlantification of the Barents Sea causes the polar front to limit the expansion of winter sea ice. *Journal of Physical Oceanography*, *48*(8), 1849–1866. https://doi.org/10.1175/JPO-D-18-0003.1

Bourgain, P., & Gascard, J.-C. (2011). The arctic ocean halocline and its interannual variability from 1997 to 2008. *Deep Sea Research Part I: Oceanographic Research Papers*, *58*(7), 745–756. https://doi.org/10.1016/j.dsr.2011.05.001

Campbell, K., Mundy, C., Landy, J., Delaforge, A., Michel, C., & Rysgaard, S. (2016). Community dynamics of bottom-ice algae in Dease Strait of the Canadian Arctic. *Progress in Oceanography*, *149*, 27–39. https://doi.org/10.1016/j.pocean.2016.10.005

Demidov, A., Gagarin, V., Artemiev, V., Arashkevich, E., Makkaveev, P., Shchuka, S., et al. (2020). Vertical variability of primary production and features of the subsurface chlorophyll maximum in the Laptev Sea in August-September, 2015, 2017, and 2018. *Oceanology*, *60*(2), 189–204. https://doi.org/10.1134/S0001437020010063

Fer, I., Koenig, Z., Kozlov, I. E., Ostrowski, M., Rippeth, T. P., Padman, L., et al. (2020). Tidally forced lee waves drive turbulent mixing along the Arctic Ocean margins. *Geophysical Research Letters*, *47*(16), e2020GL088083. https://doi.org/10.1029/2020GL088083

Fer, I., Müller, M., & Peterson, A. (2015). Tidal forcing, energetics, and mixing near the Yermak Plateau. *Ocean Science*, *11*, 287–304. https://doi.org/10.5194/os-11-287-2015

Fouest, V. L., Babin, M., & Tremblay, J.-É. (2013). The fate of riverine nutrients on Arctic shelves. *Biogeosciences*, *10*(6), 3661–3677. https://doi.org/10.5194/bg-10-3661-2013

Janout, M. A., Tippenhauer, S., Schulz, K., Mohrholz, V., Ivanov, V., & Polyakov, I. (2020). Microstructure measurements during Akademik Tryoshnikov cruise AT2018 to the Arctic Ocean. [Dataset]. PANGAEA. https://doi.org/10.1594/PANGAEA.925880

Lenn, Y.-D., Rippeth, T. P., Old, C. P., Bacon, S., Polyakov, I., Ivanov, V., & Hölemann, J. (2011). Intermittent intense turbulent mixing under ice in the Laptev Sea continental shelf. *Journal of Physical Oceanography*, *41*(3), 531–547. https://doi.org/10.1175/2010JPO4425.1

Lenn, Y.-D., Wiles, P., Torres-Valdes, S., Abrahamsen, E., Rippeth, T., Simpson, J., et al. (2009). Vertical mixing at intermediate depths in the Arctic boundary current. *Geophysical Research Letters*, *36*(5). https://doi.org/10.1029/2008GL036792

MacKinnon, J. A., Simmons, H. L., Hargrove, J., Thomson, J., Peacock, T., Alford, M. H., et al. (2021). A warm jet in a cold ocean. *Nature Communications*, *12*(1), 1–12. https://doi.org/10.1038/s41467-021-22505-5

Meyer, A., Sundfjord, A., Peterson, A. K., & Peterson, A. K. (2017). Fer, IMixing rates and vertical heat fluxes north of svalbard from arctic winter to spring. *Journal of Geophysical Research: Oceans*, *122*(6), 4569–4586. https://doi.org/10.1002/2016JC012441

Padman, L., Plueddemann, A. J., Muench, R. D., & Pinkel, R. (1992). Diurnal tides near the Yermak Plateau. *Journal of Geophysical Research: Oceans*, *97*(C8), 12639–12652. https://doi.org/10.1029/92JC01097

Pawlowicz, R. (2000). *M_Map: A mapping package for Matlab*. University of British Columbia Earth and Ocean Sciences. [Online]. Retrieved from http://www.eos.ubc.ca/rich/map.html

Pnyushkov, A. V., Polyakov, I. V., Ivanov, V. V., Aksenov, Y., Coward, A. C., Janout, M., & Rabe, B. (2015). Structure and variability of the boundary current in the Eurasian Basin of the Arctic Ocean. *Deep Sea Research Part I: Oceanographic Research Papers*, *101*, 80–97. https://doi.org/10.1016/j.dsr.2015.03.001

Polyakov, I. V., Padman, L., Lenn, Y.-D., Pnyushkov, A., Rember, R., & Ivanov, V. V. (2019). Eastern Arctic Ocean diapycnal heat fluxes through large double-diffusive steps. *Journal of Physical Oceanography*, *49*(1), 227–246. https://doi.org/10.1175/JPO-D-18-0080.1

Polyakov, I. V., Pnyushkov, A. V., Alkire, M. B., Ashik, I. M., Baumann, T. M., Carmack, E. C., et al. (2017). Greater role for Atlantic inflows on sea-ice loss in the Eurasian basin of the Arctic Ocean. *Science*, *356*(6335), 285–291. https://doi.org/10.1126/science.aai8204

Polyakov, I. V., Rippeth, T. P., Fer, I., Alkire, M. B., Baumann, T. M., Carmack, E. C., et al. (2020). Weakening of cold halocline layer exposes sea ice to oceanic heat in the eastern Arctic Ocean. *Journal of Climate*, *33*(18), 8107–8123. https://doi.org/10.1175/JCLI-D-19-0976.1

Randelhoff, A., Fer, I., Sundfjord, A., Tremblay, J.-É., & Reigstad, M. (2016). Vertical fluxes of nitrate in the seasonal nitracline of the Atlantic sector of the Arctic Ocean. *Journal of Geophysical Research: Oceans*, *121*(7), 5282–5295. https://doi.org/10.1002/2016JC011779

Randelhoff, A., Holding, J., Janout, M., Sejr, M. K., Babin, M., Tremblay, J.-E., & Alkire, M. B. (2020). Pan-Arctic Ocean primary production constrained by turbulent nitrate fluxes. *Frontiers in Marine Science*, *7*, 150. https://doi.org/10.3389/fmars.2020.00150

Renner, A., Sundfjord, A., Janout, M., Ingvaldsen, R. B., Beszczynska-Möller, A., Pickart, R. S., & Pérez-Hernández, M. D. (2018). Variability and redistribution of heat in the Atlantic water boundary current north of Svalbard. *Journal of Geophysical Research: Oceans*, *123*(9), 6373–6391. https://doi.org/10.1029/2018JC013814

Rippeth, T. P., Lincoln, B. J., Lenn, Y.-D., Green, J. M., Sundfjord, A., & Bacon, S. (2015). Tide-mediated warming of Arctic halocline by Atlantic heat fluxes over rough topography. *Nature Geoscience*, *8*(3), 191–194. https://doi.org/10.1038/ngeo2350

Rippeth, T. P., Vlasenko, V., Stashchuk, N., Scannell, B. D., Green, J. M., Lincoln, B. J., & Bacon, S. (2017). Tidal conversion and mixing poleward of the critical latitude (an Arctic case study). *Geophysical Research Letters*, *44*(24), 12–349. https://doi.org/10.1002/2017GL075310

Rudels, B. (2012). Arctic Ocean circulation and variability-advection and external forcing encounter constraints and local processes. *Ocean Science*, *8*, 261–286. https://doi.org/10.5194/os-8-261-2012

Sakamoto, C. M., Johnson, K. S., & Coletti, L. J. (2009). Improved algorithm for the computation of nitrate concentrations in seawater using an in situ ultraviolet spectrophotometer. *Limnology and Oceanography: Methods*, *7*(1), 132–143. https://doi.org/10.4319/lom.2009.7.132

Schauer, U., Muench, R. D., Rudels, B., & Timokhov, L. (1997). Impact of eastern Arctic shelf waters on the Nansen Basin intermediate layers. *Journal of Geophysical Research: Oceans*, *102*(C2), 3371–3382. https://doi.org/10.1029/96JC03366

Schulz, K., Büttner, S., Rogge, A., Janout, M., Hölemann, J., & Rippeth, T. P. (2021). Turbulent mixing and the formation of an intermediate nepheloid layer above the Siberian continental shelf break. *Geophysical Research Letters*, *48*, e2021GL092988. https://doi.org/10.1029/2021GL092988

Schulz, K., Janout, M., Lenn, Y.-D., Ruiz-Castillo, E., Polyakov, I., Mohrholz, V., et al. (2021). On the along-slope heat loss of the boundary current in the Eastern Arctic Ocean. *Journal of Geophysical Research: Oceans*, *126*(2), e2020JC016375. https://doi.org/10.1029/2020JC016375

Stroeve, J., Serreze, M., Drobot, S., Gearheard, S., Holland, M., Maslanik, J., et al. (2008). Arctic sea ice extent plummets in 2007. *Eos, Transactions American Geophysical Union*, *89*(2), 13–14. https://doi.org/10.1029/2008EO020001

Tarasenko, A., Supply, A., Kusse-Tiuz, N., Ivanov, V., Makhotin, M., Tournadre, J., et al. (2021). Surface waters properties in the Laptev and the East-Siberian Seas in summer 2018 from in situ and satellite data. *Ocean Science*, *17*(1), 221–247. https://doi.org/10.5194/os-17-221-2021

Torres-Valdés, S., Tsubouchi, T., Bacon, S., Naveira-Garabato, A. C., Sanders, R., McLaughlin, F. A., et al. (2013). Export of nutrients from the Arctic Ocean. *Journal of Geophysical Research: Oceans*, *118*(4), 1625–1644. https://doi.org/10.1002/jgrc.20063

Tremblay, J.-E., Anderson, L. G., Matrai, P., Coupel, P., Bélanger, S., Michel, C., & Reigstad, M. (2015). Global and regional drivers of nutrient supply, primary production and $CO_2$ drawdown in the changing Arctic Ocean. *Progress in Oceanography*, *139*, 171–196. https://doi.org/10.1016/j.pocean.2015.08.009